



## Measurement of the forward-backward asymmetry in $p\bar{p} \rightarrow t\bar{t}$ production in the $l+\text{jets}$ channel

The DØ Collaboration  
URL <http://www-d0.fnal.gov>  
(Dated: March 13, 2014)

We present a measurement of the forward–backward asymmetry in top quark–antiquark production using the full Tevatron Run II dataset collected by the D0 experiment at Fermilab. The measurement is performed in lepton+jets final states using a new kinematic fitting algorithm for events with four or more jets and a new partial reconstruction algorithm for events with only three jets. When corrected for detector acceptance and resolution effects the asymmetry is evaluated to be  $A_{\text{FB}} = (10.6 \pm 3.0)\%$ . We also present the dependence of the asymmetry on the invariant mass of the  $t\bar{t}$  system. Results are compatible with standard model predictions that range from 5.0% to 8.8%.

## I. INTRODUCTION

### A. Motivation and definitions

Over the last five years both experiments at the Fermilab Tevatron Collider measured positive forward–backward asymmetries in the production of top quark–antiquark pairs in proton–antiproton collisions ( $p\bar{p} \rightarrow t\bar{t}$ ) [1–5]. The reported values were consistently above predictions of the standard model of particle physics (SM) [6, 7]. In particular, the CDF Collaboration observed a strong rise of the asymmetry with the invariant mass of the  $t\bar{t}$  system,  $m_{t\bar{t}}$  [3]. The dependence of the asymmetry on  $m_{t\bar{t}}$  in D0 data, as measured in Ref. [4], was statistically compatible with both the SM predictions and with the CDF result. Several beyond-the-SM scenarios were suggested to explain the measured  $A_{\text{FB}}$  values (e.g. Refs. [8, 9]). In this note we report new results from the D0 experiment based on the full dataset collected during Run II of the Fermilab Tevatron Collider, which supersede the result of Ref. [4].

In proton–antiproton collisions, top quark–antiquark ( $t\bar{t}$ ) pairs are predominantly produced via valence quark–antiquark annihilation. Thus, the direction of the proton (antiproton) almost always coincides with the direction of the incoming quark (antiquark). We define the difference in rapidity<sup>1</sup> between the top quark ( $y_t$ ) and antiquark ( $y_{\bar{t}}$ ):

$$\Delta y = y_t - y_{\bar{t}}. \quad (1)$$

We refer to the events that have  $\Delta y > 0$  as “forward”, and to those with  $\Delta y < 0$  as “backward”. The forward–backward asymmetry in  $t\bar{t}$  production is defined as

$$A_{\text{FB}} = \frac{N_f - N_b}{N_f + N_b}, \quad (2)$$

where  $N_f$  ( $N_b$ ) is the number of forward (backward) events. All the  $t\bar{t}$  asymmetries reported in this note are after the subtraction of the contributions due to background processes.

The rapidities of the  $t$  and  $\bar{t}$  quarks and the corresponding asymmetries can be defined at the production level (sometimes denoted as generator level, or parton level), when the kinematic parameters of the generated top quarks are used. Unless stated otherwise the production-level asymmetries are reported without imposing the selection criteria of this analysis. The rapidities and asymmetry can also be defined at the reconstruction level, using the reconstructed kinematics of the selected events. Similarly, the invariant mass of the  $t\bar{t}$  system can be defined at the production and reconstruction levels.

### B. Strategy

To identify  $t\bar{t}$  events in the  $t\bar{t} \rightarrow W^+bW^-\bar{b}$ ;  $W^+ \rightarrow l^+\nu_l$ ;  $W^- \rightarrow q\bar{q}'$  (and charge conjugates) decay chain we select events that contain one isolated lepton (electron or muon) of high transverse momentum ( $p_T$ ) and at least three jets. This channel is commonly referred to as the “lepton+jets” ( $l$ +jets) channel. The electric charge of the lepton identifies the electric charge of the “leptonically decaying top quark”. The hadronically decaying top quark is assumed to have the opposite charge. The event selection, sample composition determination, and modeling of the signal and background processes are identical to those used in the measurement of the leptonic asymmetry in  $t\bar{t}$  production in the  $l$ +jets channel [10]. The four-vectors of the top quarks and antiquarks in the events containing at least four jets are reconstructed with a kinematic fitting algorithm, while for the events that contain only three jets a partial reconstruction algorithm is used. If a jet exhibits properties consistent with a jet originating from a  $b$  quark, such as the presence of a reconstructed secondary vertex, we call it a  $b$ -tagged jet [12]. The  $l$ +jets events are separated into channels defined by jet and  $b$ -tag multiplicities. The amount of signal and the forward-backward asymmetry at the reconstruction level are determined using a simultaneous fit to a kinematic discriminant in these channels.

The measured background-subtracted one-dimensional (1D) distribution in  $\Delta y$  is corrected to the production level (“unfolded”). To study the dependence of the asymmetry on the invariant mass of the  $t\bar{t}$  system, unfolding is done on the background-subtracted data distributions in two dimensions (2D:  $\Delta y$  vs  $m_{t\bar{t}}$ ). The signal channels are unfolded simultaneously to yield the desired 1D or 2D production-level distributions, from which the production-level  $A_{\text{FB}}$  values are computed using Eq. 2. The procedure is calibrated using simulated samples with varied asymmetries and input distributions in  $\Delta y$  and  $m_{t\bar{t}}$ . The statistical and systematic uncertainties of the results are evaluated using ensembles of simulated pseudo-datasets.

---

<sup>1</sup> The rapidity  $y$  is defined as  $y = \frac{1}{2} \ln[(E + p_z)/(E - p_z)]$ , where  $E$  is the particle’s energy and  $p_z$  is its momentum along the  $z$ -axis, which corresponds to the direction of the incoming proton.

## II. D0 DETECTOR

We use the data collected by the D0 detector during Run II of the Tevatron in the years 2001–2011. After imposing event quality requirements ensuring that all detector systems were fully operational, this dataset corresponds to an integrated luminosity of  $9.7 \text{ fb}^{-1}$ . The D0 detector is described in detail elsewhere [13]. The central tracking system, consisting of a silicon microstrip tracker and a scintillating fiber tracker, is enclosed within a 1.9 T superconducting solenoid magnet. Tracks of charged particles are reconstructed within a pseudorapidity region<sup>2</sup> of  $|\eta| < 2.5$ . Electrons, photons, and jets of hadrons are identified using a liquid-argon and uranium-plate calorimeter, which consists of a central barrel covering up to  $|\eta| \approx 1.1$ , and two endcap sections that extend coverage to  $|\eta| \approx 4.2$  [14]. Central and forward preshower detectors are positioned in front of the corresponding sections of the calorimeter. A muon system consisting of layers of tracking detectors and scintillation counters placed in front of and behind 1.8 T iron toroids [15] identifies muons within  $|\eta| < 2$ . Luminosity is measured using arrays of plastic scintillators located in front of the endcap calorimeter cryostats. A three-level trigger system selects interesting events at the rate of 200 Hz for offline analysis [16].

## III. EVENT RECONSTRUCTION AND SELECTION

Object reconstruction and identification, as well as event selection, are the same as in Ref. [10] and are briefly outlined in this section. We select events with exactly one isolated electron within the pseudorapidity range of  $|\eta| < 1.1$  or one isolated muon within  $|\eta| < 2.0$ , and at least three jets within  $|\eta| < 2.5$ . Leptons of either flavor are required to have  $|y| < 1.5$ . The presence of a neutrino is inferred from a transverse momentum imbalance, which is measured primarily using calorimetry and is referred to as “the missing transverse energy”, or  $\cancel{E}_T$ . All objects have transverse momentum  $p_T > 20 \text{ GeV}$ , and the jet with the largest  $p_T$  (the leading jet) is also required to have  $p_T > 40 \text{ GeV}$ .

To identify jets that are likely to be associated with  $b$  quarks, we perform a multivariate analysis (*MVA*) that combines variables characterizing the properties of secondary vertices and of tracks with large impact parameters relative to the primary  $p\bar{p}$  interaction vertex (PV) [12]. The output of the *MVA* is a continuous variable  $MVA_b$ . The cut on  $MVA_b$  used in this analysis has an efficiency of about 64% for identifying  $b$  jets originating from top quark decay, and a misidentification probability of about 7% for jets that do not contain heavy flavor quarks and are produced in association with  $W$  bosons.

Events are divided into six channels by the number of jets and  $b$  tags:  $l+3\text{jet}$  and  $l+\geq 4\text{jet}$  with 0, 1, and  $\geq 2$   $b$  tags each. The three-jet zero- $b$ -tag channel is used only for the background asymmetry calibration, and not for the  $t\bar{t}$  asymmetry measurement. The four-jet zero- $b$ -tag channel is used only for determining the sample composition and the reconstruction-level  $A_{\text{FB}}$ , and is not used for measuring the production-level asymmetry.

For  $l+\geq 4\text{jet}$  events, the  $t\bar{t}$  system is fully reconstructed using a kinematic fitting algorithm. Previous D0 top quark analyses used the algorithm of Ref. [17]. In this note a new algorithm is employed, which utilizes an analytic solution for the neutrino momentum using the constraints on the  $W$ -boson and top-quark masses [18]. The likelihood of each possible assignment of the observed objects to the  $t\bar{t}$  decay products is calculated. The likelihood term for each of the four jets with the largest  $p_T$  accounts for the differences between the observed jet energy and the energy scaled to satisfy the constraints on the masses of the  $W$  boson and top quark. The jet energy resolution and the probability for a jet to be reconstructed (see “Type III” transfer function in Ref. [19]) are taken into account. The  $b$ -tagging observables  $MVA_b$  are also used to evaluate the likelihood of each assignment.

For  $l+3\text{jet}$  events, a partial reconstruction algorithm of the  $t\bar{t}$  decay chain is employed [11]. With one jet entirely lost, there is little to gain from scaling the four-vectors of the remaining objects as is done by the kinematic fitting algorithm in  $l+\geq 4\text{jet}$  events, so the partial reconstruction algorithm does not attempt to modify the observed objects. As only the transverse components of the neutrino momentum are measured in  $\cancel{E}_T$ , the longitudinal component is calculated from the known  $W$  boson mass in the  $W \rightarrow l\nu$  decay, which results in a quadratic equation. The two-fold ambiguity is resolved by picking the solution that minimizes the difference between the invariant mass of the objects assigned to the leptonic top quark decay and the known top quark mass. Thus, this algorithm assumes that the jet associated with the  $b$  quark from the leptonically decaying top quark is present. This assumption holds for 80% of the  $t\bar{t}$  events. The lost jet is assumed to be either the jet associated with the  $b$  quark from the hadronic top

---

<sup>2</sup> The pseudorapidity  $\eta$  is defined as  $-\ln \left[ \tan \left( \frac{\theta}{2} \right) \right]$ , where  $\theta$  is the polar angle. The angle  $\theta = 0$  corresponds to the direction of the incoming proton.

quark decay, or a jet associated with a light quark from the hadronically decaying  $W$  boson. In the majority of the cases (74%) this jet is lost due to its low energy, so this loss has only a small effect on the kinematics of the hadronically decaying top quark. In the partial reconstruction algorithm the lost jet is neglected. The sum of the four-vectors of the two jets assigned to the products of the hadronically decaying top quark serves as a proxy for the four-vector of the hadronically decaying top quark. Even though the reconstructed invariant mass of the proxy is not expected to be equal to the top quark mass, its distribution is different for combinations correctly associated with the hadronically decaying top quark and combinations that include a  $b$  jet from the leptonically decaying top quark. In each event we consider the following nine observables: the  $MVA_b$  values for each of the three jets, the three possible mass combinations of the leptonically decaying top quark,  $m_l$ , and the three possible proxy masses,  $m_p$ . There are three possible jet-to-quark assignments, corresponding to the three possible choices for the jet from the leptonic top quark decay. The likelihood of each assignment is calculated by evaluating the consistency of the nine observables with the distributions corresponding to the hypothesized assignment. In particular, the jet hypothesized to be associated with a  $b$  quark should have a value of  $MVA_b$  consistent with the one expected for  $b$  jets, while for a jet hypothesized to originate from a  $W$  boson decay this observable should be consistent with the distribution expected for such jets. The values of  $m_l$  and  $m_p$  for the jet combinations that correspond to the hypothesized assignment should be consistent with the distributions expected for correctly assigned jets, while the values of  $m_l$  and  $m_p$  for the other jet combinations should agree with the distributions expected for wrong assignments. When calculating the invariant mass of the  $t\bar{t}$  system, we compensate for the effect of the lost jet by applying an  $m_p$ -dependent scaling to the four-vector of the hadronically decaying top quark.

Unlike the  $A_{\text{FB}}$  measurement in Ref. [4], where only the jet-to-quark assignment with the lowest  $\chi^2$  was used, in this analysis we reconstruct  $\Delta y$  by averaging its values over all possible assignments, weighted by their likelihoods evaluated as described above for  $l+\geq 4$  jet and  $l+3$  jet events. The same approach is used to reconstruct  $m_{t\bar{t}}$  in the  $l+3$  jet channel. For  $l+\geq 4$  jet events,  $m_{t\bar{t}}$  is reconstructed using the outputs of three reconstruction algorithms: the new kinematic fit algorithm, the kinematic fit algorithm of Ref. [17], and a simple reconstruction [20], which evaluates the kinematics of the leptonically decaying  $W$  boson from the lepton and the neutrino by imposing the  $W$ -boson mass constraint and calculates  $m_{t\bar{t}}$  by adding the four most energetic jets without imposing the top-quark mass constraint. All this information, and supplementary observables such as the mass of the leading jet, are combined using a multivariate regression [21] to yield a reconstruction of  $m_{t\bar{t}}$  which combines the benefits of the individual input algorithms for all  $m_{t\bar{t}}$  ranges.

For the asymmetry measurement the performance of a  $t\bar{t}$  reconstruction algorithm can be characterized by the probability to correctly reconstruct the sign of  $\Delta y$ ,  $P(\text{correct sign})$ , which is shown in Fig. 1 as a function of the production-level  $|\Delta y|$  for three different algorithms. For the algorithm employed in this analysis for  $l+\geq 4$  jet events the overall  $P(\text{correct sign})$  is 77.5%, compared to 75.6% for the algorithm of Ref. [17]. The partial reconstruction algorithm correctly identifies the sign of  $\Delta y$  in 74.5% of  $l+3$  jet events. The surprisingly high probability for  $l+3$  jet events can be understood from the following consideration. All four leading jets are associated with the quarks from the  $t\bar{t}$  decay in only 55% of the  $l+\geq 4$  jet events. For the other 45% of the events one of the jets originates from initial or final state radiation, which can lead to badly misreconstructed  $t\bar{t}$  four-vectors. Only 4% of the  $l+3$  jet events contain a jet that does not originate from the  $t\bar{t}$  decay. Thus, even though some information is lost with the unreconstructed jet, no wrong information is added, leading to fewer migrations between the event categories.

#### IV. SM PREDICTIONS

Until recently the differential cross section for  $t\bar{t}$  production was calculated only at order  $\alpha_s^3$ , where  $\alpha_s$  is the strong coupling constant. Since in the SM the  $t\bar{t}$  asymmetry only appears at this order, no full higher order prediction for the effect exists yet. The relative uncertainty on the  $\alpha_s^3$  calculation of the asymmetry due to higher order corrections is evaluated to be as large as  $\approx 25\%$  [22].

Recently the order  $\alpha_s^4$  calculation for the total cross section of  $t\bar{t}$  production [23] was made available, but the asymmetry was not computed at this order. Several papers report calculations of the leading corrections to the asymmetry with the predicted  $A_{\text{FB}}$  values ranging from 5.0% in MC@NLO [24] to 8.8% once the electroweak corrections [25] and resummations of particular corners of phase space [26] are taken into account. The dominant uncertainty on these predictions is from the renormalization and factorization scales, and is evaluated to be up to 2.0% [22, 27]. The authors of Ref. [28] obtain a value of  $A_{\text{FB}} = 12.7\%$  by employing a normalization scale that arguably stabilizes the perturbative expansion yet differs significantly from the scales commonly used in top quark physics calculations. Some authors suggest that the corrections from interactions between the top quark decay products and the proton remnants should be taken into account when calculating  $A_{\text{FB}}$  [29].

Given this variety of predictions, we choose to compare our data to the well defined MC@NLO simulation (version 3.4) with the parton showering performed by HERWIG [30]. This simulation is fully integrated in D0 software, allowing

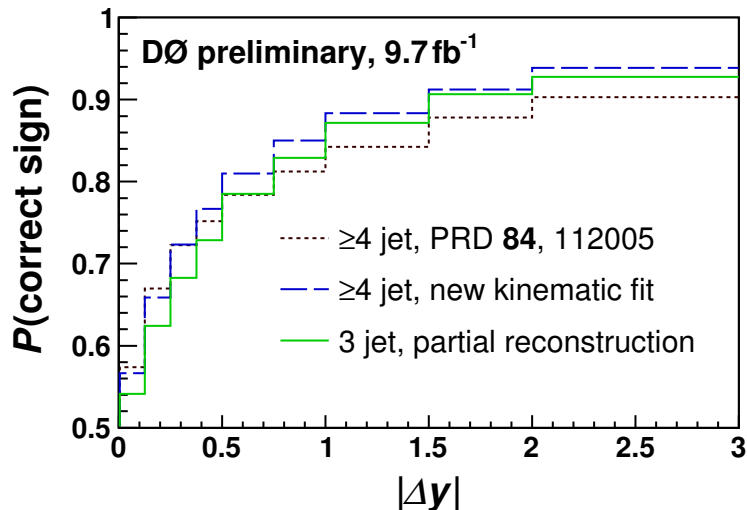


FIG. 1:  $P(\text{correct sign})$  as a function of the production-level  $|\Delta y|$  for the algorithm of Ref. [17] used to measure the  $A_{\text{FB}}$  in Ref. [4] and the algorithms used to reconstruct  $l+\geq 4\text{jet}$  events and to partially reconstruct  $l+3\text{jet}$  events in this note.

for detailed studies of the kinematic dependences of  $A_{\text{FB}}$  and their interplay with selection and reconstruction effects. MC@NLO predicts an overall asymmetry in  $t\bar{t}$  production before selection of  $5.01 \pm 0.03\%$ . Here and in the following sections the quoted uncertainties on the predictions are from the finite size of the simulated samples unless otherwise stated.

At order  $\alpha_s^3$ , the QCD contributions to the asymmetry in  $t\bar{t}$  production can be divided into two classes up to divergences that cancel between these two classes [6]. The first class that contributes to negative asymmetry, is a result of an interference between the terms that contain gluon radiation in the initial or final states, which may result in an extra jet in the event and typically leads to a higher momentum of the  $t\bar{t}$  system. The second class, which contributes to positive asymmetry, is an interference between the Born term ( $\alpha_s^2$ ) and the term described by a box diagram ( $\alpha_s^4$ ). The overall asymmetry is positive and depends on the jet multiplicity. Selection criteria that give preference to events with higher jet multiplicity favor the first class of events and thus lower the overall expected asymmetry, while a higher asymmetry is expected for events with lower jet multiplicity. Consequently, forward events tend to have fewer jets than events in the backward category. Similarly, since a  $b$ -tagged jet is less likely to originate from initial or final state radiation, samples with a larger number of  $b$  tags tend to have higher values of  $A_{\text{FB}}$ . Table I lists the MC@NLO predictions for  $t\bar{t}$  events after the selection criteria are applied.

All previous measurements of  $A_{\text{FB}}$  in the  $l+\text{jets}$  channel selected  $t\bar{t}$  events that had at least four jets in the final state. As is apparent from Table I these events have lower production-level asymmetry than the overall predicted value. By including events with three jets, this selection bias is reduced, leading to smaller acceptance corrections.

TABLE I: Asymmetries predicted by MC@NLO for  $t\bar{t}$  events that pass the analysis selection criteria. Statistical uncertainties only.

Channel	$A_{\text{FB}}, \%$	
	Production level	Reconstruction level
$\geq 3$ jets, $\geq 1$ $b$ tags	$4.7 \pm 0.1$	$3.9 \pm 0.1$
3 jets, 1 $b$ tag	$6.6 \pm 0.2$	$4.7 \pm 0.3$
3 jets, $\geq 2$ $b$ tags	$7.3 \pm 0.2$	$5.6 \pm 0.2$
$\geq 4$ jets, 1 $b$ tag	$1.4 \pm 0.2$	$1.9 \pm 0.2$
$\geq 4$ jets, $\geq 2$ $b$ tags	$3.2 \pm 0.1$	$3.3 \pm 0.2$

Asymmetries after reconstruction are presented in the last column of Table I. Finite resolution in  $\Delta y$  results in roughly 20% of the forward events being misreconstructed as backward, and vice versa. Since there are more forward events,  $\Delta y$  smearing leads to an overall lowering of the reconstructed asymmetries. At the same time, forward  $t\bar{t}$  events, which tend to have fewer jets, have a lower probability to be misreconstructed, resulting in fewer migrations into the backward category, and an upward shift in the reconstructed asymmetry. This bias is most apparent in the  $l+\geq 4\text{jet}$ , one- $b$ -tag channel, where the lowest asymmetry is predicted.

## V. SAMPLE COMPOSITION AND RECONSTRUCTION-LEVEL $A_{\text{FB}}$

The main source of background to  $t\bar{t}$  signal is the production of a leptonically decaying  $W$  boson in association with jets ( $W$ +jets). The kinematic properties of this process are simulated using ALPGEN [31] with hadronic showering performed by PYTHIA [32]. For signal and background modeling we use the CTEQ6.1 set of parton distribution functions (PDFs) [33]. The normalization of the  $W$ +jets contribution is a free parameter in the fitting procedure described below. Events with multiple jets can also mimic  $t\bar{t}$  signal when a particle within one of the jets is misidentified as an isolated lepton. The normalization of this multijet background is extrapolated from a control sample enriched in this process using the probability for a jet to satisfy the lepton-quality requirements [34]. For the other backgrounds,  $Z$ +jets events are simulated with ALPGEN, diboson events are simulated with PYTHIA, and events from single-top-quark production are simulated with COMPHEP [35]. The normalizations for the last three background processes are taken from NLO calculations [36]. For all simulated events, event generation is followed by the D0 detector simulation and reconstruction programs.

Several variables that have different distributions for signal and background processes, and that have minimal correlations between each other and with  $\Delta y$  and  $m_{t\bar{t}}$ , are combined into a kinematic discriminant bound between zero and one [10]. For  $l+\geq 4$  jet events a discriminant  $D_4$  is built from the following input variables:

- $\chi^2$  – the test statistic of the likeliest assignment from the kinematic fit.
- $p_T^{\text{LB}}$  – the transverse momentum of the leading  $b$ -tagged jet, or when no jets are  $b$  tagged, the  $p_T$  of the leading jet.
- $k_T^{\text{min}}$  =  $\min(p_{T,a}, p_{T,b}) \cdot \Delta\mathcal{R}_{ab}$ , where  $\Delta\mathcal{R}_{ab} = \sqrt{(\eta_a - \eta_b)^2 + (\phi_a - \phi_b)^2}$  is the angular distance between the two closest jets,  $a$  and  $b$ , and  $p_{T,a}$  and  $p_{T,b}$  are their transverse momenta.
- $M_{jj}$ , the invariant mass of the jets assigned to the  $W \rightarrow q\bar{q}'$  decay in the kinematic fit, calculated using kinematic quantities before the fit.

The variables  $\chi^2$  and  $M_{jj}$  are based on the full  $t\bar{t}$  reconstruction using the kinematic fitting technique of Ref. [17].

For the  $l+3$  jet channels we construct a discriminant  $D_3$  using a different set of input variables:

- $S$  – the sphericity [37], defined as  $S = \frac{3}{2}(\lambda_2 + \lambda_3)$ , where  $\lambda_2$  and  $\lambda_3$  are the two highest out of the three eigenvalues of the normalized quadratic momentum tensor  $M$ . The tensor  $M$  is defined as

$$M_{ij} = \frac{\sum_o p_i^o p_j^o}{\sum_o |p^o|^2}, \quad (3)$$

where  $p^o$  is the momentum vector of a reconstructed object  $o$ , and  $i$  and  $j$  run over the three indices for the Cartesian coordinates. The sum over objects includes the three selected jets and the selected charged lepton.

- $p_T^{3^{\text{rd}}}$  – the transverse momentum of the third leading jet.
- $M_{jj}^{\text{min}}$  – the lowest of the invariant masses of two jets, out of the three possible jet pairings.
- $p_T^{\text{LB}}$ , defined as for the  $l+\geq 4$  jet channel, above.
- $\Delta\phi(\text{jet}_1, \cancel{E}_T)$ , the difference in azimuthal angle between the leading jet and the transverse momentum imbalance.

Given the number of  $b$ -tagged jets,  $N_b$ , which is truncated at two, the discriminants for all channels are concatenated into a single discriminant  $D_c$ , so that for the  $l+3$  jet events  $D_c = N_b + D_3$ , while for  $l+\geq 4$  jet events  $D_c = 3 + N_b + D_4$ . We fit the sum of the signal and background templates to the data distribution in the discriminant  $D_c$  as shown in Fig. 2. This fit is identical to the fit for the sample composition in Ref. [10]. The sample composition and its breakdown into individual channels is summarized in Table II. Background contributions other than  $W$ +jets and multijet production are labeled “Other bg” in Table II.

In the simulated  $W$ +jets background, the angular distribution of leptons from  $W$ -boson decay has a forward-backward asymmetry [38]. Due to this asymmetry, when these events are reconstructed according to the  $t\bar{t}$  hypothesis, there remains a residual asymmetry in the  $\Delta y$  distribution. To improve the modeling of this asymmetry, we apply to each simulated  $W$ +jets event a weight dependent on the product of the generated lepton charge and its rapidity. These weights are chosen so that the simulation best matches control data with three jets and zero  $b$  tags as in Ref. [10]. The difference in the  $\Delta y$  distributions predicted by the simulation with and without the applied weights is treated as a source of systematic uncertainty due to background modeling. This uncertainty exceeds the uncertainty due to

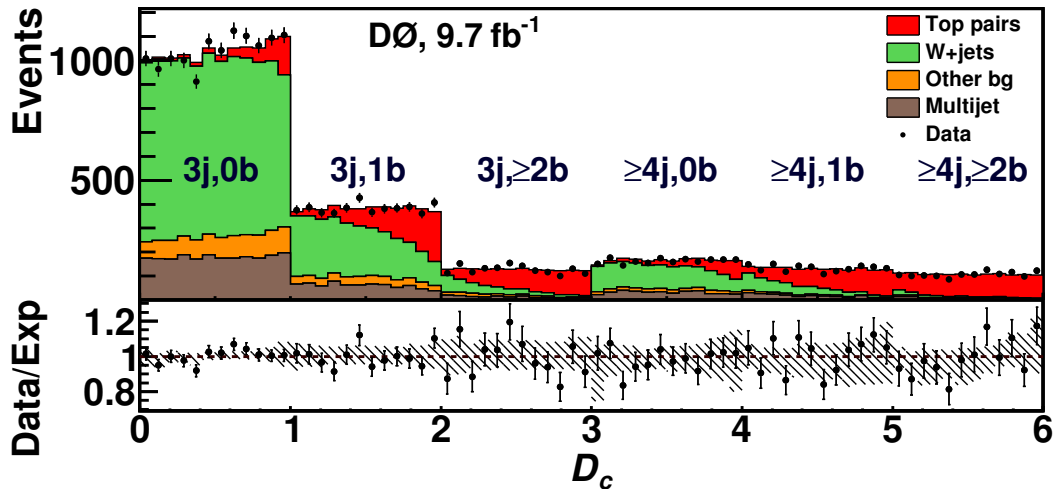


FIG. 2: The combined discriminant  $D_c$ . The region  $D_c < 1$  is not used to determine the signal  $A_{FB}$ . The ratio between the data counts and the model expectation is shown in the lower panel, with the hashed area representing the systematic uncertainties. Figure is from Ref. [10].

TABLE II: Estimated number of events from the fit of the data distribution in the discriminant  $D_c$  to the sum of signal and background processes. The sum of the estimated number of signal and background events is constrained to be equal to that in data. The second column includes events with zero  $b$  tags. The statistical uncertainties from the fit are quoted. Table is from Ref. [10].

Source	Selected	3 jets		$\geq 4$ jets	
	events	1 $b$ tag	$\geq 2$ $b$ tags	1 $b$ tag	$\geq 2$ $b$ tags
W+jets	$4447 \pm 74$	2461	352	403	79
Multijet	$969 \pm 24$	449	95	127	62
Other bg	786	404	112	75	32
Signal	$4745 \pm 70$	1212	1001	983	1166
Sum	10947	4526	1560	1588	1339
Data	10947	4588	1527	1594	1281

PDFs by about a factor of two. We rely on the simulation to predict the variation of the asymmetry with jet and  $b$ -tag multiplicities.

The distributions of the reconstructed  $\Delta y$  are shown in Fig. 3. The  $t\bar{t}$  asymmetry at the reconstruction level is extracted using a fit to the distributions in the discriminant  $D_c$  and sign of  $\Delta y$ , excluding the  $l+3$  jet events with zero  $b$  tags. This fitting procedure is identical to the procedure used in Ref. [10]. The inclusive asymmetry measured at the reconstruction level is  $(7.9 \pm 2.1(\text{stat})_{-0.9}^{+0.8}(\text{syst}))\%$ . The results for individual channels are listed in Table III.

TABLE III: Reconstruction-level background-subtracted asymmetries for selected events for different channels. The last line includes the channels listed above and the  $\geq 4$  jet, zero- $b$ -tag channel. The first uncertainty is statistical, and the second one is systematic. Systematic uncertainties are discussed in Section VII. The prediction is based on the MC@NLO simulation.

Channel	$A_{FB}, \%$	
	Predicted	Measured
3 jets, 1 $b$ tag	4.7	$5.4 \pm 6.0_{-4.0}^{+3.3}$
3 jets, $\geq 2$ $b$ tags	5.6	$10.7 \pm 4.2 \pm 0.8$
$\geq 4$ jets, 1 $b$ tag	1.9	$11.0 \pm 4.4 \pm 0.8$
$\geq 4$ jets, $\geq 2$ $b$ tags	3.3	$5.9 \pm 3.3 \pm 0.1$
Combined	3.9	$7.9 \pm 2.1_{-0.9}^{+0.8}$

The distributions of the reconstructed invariant mass of the  $t\bar{t}$  system are shown in Fig. 4. Since the three- and four-jet channels have different response (both mean and shape) for the invariant mass of the  $t\bar{t}$  system, the dependence of the forward-backward asymmetry on  $m_{t\bar{t}}$  at the reconstruction level is difficult to interpret and is not presented

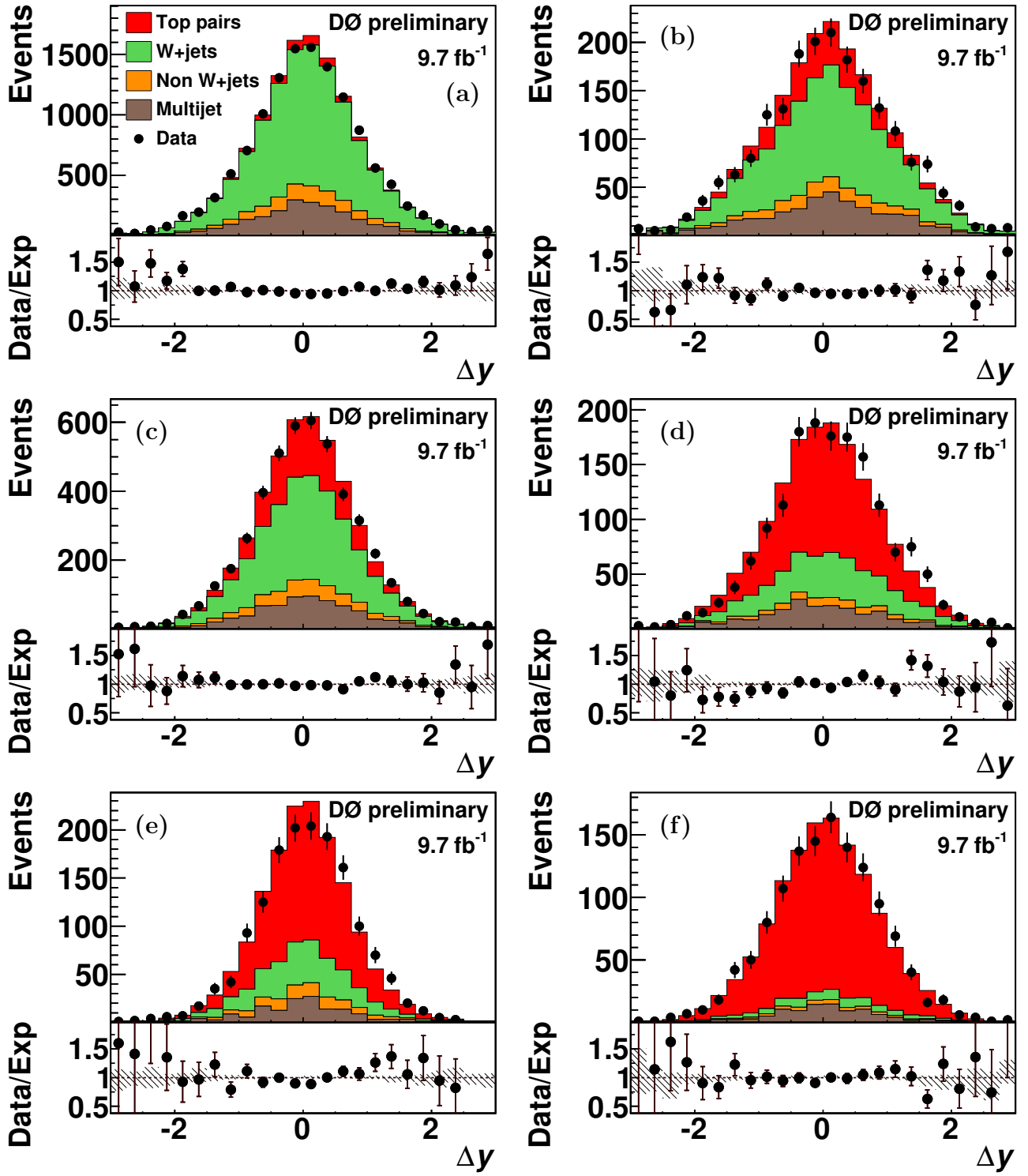


FIG. 3: Reconstructed difference between the rapidities of the top and antitop quarks,  $\Delta y$ . The left column displays  $l+3\text{jet}$  events, and the right column displays  $l+\geq 4\text{jet}$  events. Rows from top to bottom display events with 0, 1, and  $\geq 2$   $b$  tags. The ratio between the data counts and the model expectation is shown in the lower panel, with the hashed area representing the systematic uncertainties.

here. The measurement of production-level  $A_{\text{FB}}$  and its dependence on  $m_{t\bar{t}}$  is described in Section VI.

We use the results of the sample composition study summarized in Table II to normalize the distributions for the background processes in the sensitive variables ( $\Delta y$ , and for the 2D measurement also  $m_{t\bar{t}}$ ), which are subtracted from the distributions observed in data. These distributions in the four channels that contain at least one  $b$  tag are then used as inputs to the unfolding procedure.

## VI. UNFOLDING THE ASYMMETRY

The true or generated distribution of a certain variable ( $\Delta y$  for the inclusive measurement) is shaped by acceptance and detector resolution, resulting in the observed distribution, which is also subject to statistical fluctuations. The goal of the unfolding procedure is to find the best estimator for the true distribution given the background-subtracted data and knowing detector acceptance and resolution from simulation. After finding the best estimator for the true distribution of  $\Delta y$  we summarize it into  $A_{\text{FB}}$ , which is the same general approach used in the previous measurement [4]. For this unfolding we use TUNFOLD [39], which we extend as needed.

Each distribution is presented as event counts in a binned histogram, or in other words, as a vector with a dimension equal to the number of bins. Given the vector of production-level  $t\bar{t}$  signal counts  $p$  and the vector of expected background counts  $b$ , the expected data counts in  $i$ -th bin  $\tilde{d}_i$  is given by

$$\tilde{d}_i = \mathbf{T}_{ij}p_j + b_i, \quad (4)$$

$$\mathbf{T} = \mathbf{M}\mathbf{A}, \quad (5)$$

where  $\mathbf{A}$  is a diagonal acceptance matrix, whose  $jj$ -th element is the probability for an event produced in the  $j$ -th bin to pass the selection criteria and  $\mathbf{M}$  is the normalized migration matrix, whose  $ij$ -th element is the probability for a selected event produced in the  $j$ -th bin to be observed in the  $i$ -th bin.

Given the vector of observed counts  $d$  we can construct the vector of background-subtracted reconstruction-level counts  $r = d - b$  with its covariance error matrix  $\mathbf{V}$ , which takes into account the expected statistical uncertainties on data and background, in particular those due to the size of the MJ-enriched control sample.

Given the vector  $r$  we seek to find the vector  $u$ , which best estimates the vector of production-level counts  $p$  by minimizing

$$\chi^2 = (r - \mathbf{T}u)^T \mathbf{V}^{-1} (r - \mathbf{T}u) + \tau^2 (\mathbf{L}u)^T \mathbf{L}u, \quad (6)$$

where  $\tau$  is the regularization strength and  $\mathbf{L}$  is the regularization matrix. The first term of Eq. 6 quantifies the consistency of  $u$  with data, while the second (regularization) term quantifies the smoothness of  $u$ .

Without regularization, an unfolding of the data amounts to a minimization of the first term in Eq. 6. If the numbers of reconstruction- and production-level bins are equal, the problem of minimization is solved by simply inverting the matrix:  $u_{\text{unregularized}} = \mathbf{T}^{-1}r$ .

Unregularized matrix inversion typically results in unphysical, unsmooth distributions [40]. For such distributions the  $\chi^2$  is increased due to the second term of Eq. 6, which depends on the discrete second derivative of the binned distribution  $u$ . For constant bin widths, the second term is calculated using a regularization matrix with the following structure [39]:

$$\mathbf{L} = \begin{pmatrix} 0 & 0 & 0 & 0 & \dots & 0 \\ 1 & -2 & 1 & 0 & \dots & 0 \\ 0 & 1 & -2 & 1 & \dots & 0 \\ \vdots & & \ddots & \ddots & \ddots & \vdots \\ 0 & \dots & 0 & 1 & -2 & 1 \\ 0 & \dots & 0 & 0 & 0 & 0 \end{pmatrix}. \quad (7)$$

For this analysis we modify the structure of  $\mathbf{L}$  to regularize based on the second derivative of the event density rather than the event counts, which allows us to use variable bin sizes. The regularization strength  $\tau$  is chosen using both ensemble testing (described below) and the L-curve technique [39] to balance the minimization of statistical fluctuations and bias. The difference between the two techniques is included in the evaluation of the systematic uncertainty due to the choice of the regularization strength.

As in Ref. [4], the production-level  $\Delta y$  distribution is divided into 26 bins and the reconstruction-level  $\Delta y$  distribution is divided into 50 bins. Both have narrower bins near  $\Delta y = 0$ , where the probability to misclassify forward events as backward or vice versa changes rapidly and wider bins at high  $|\Delta y|$ , where statistics are low.

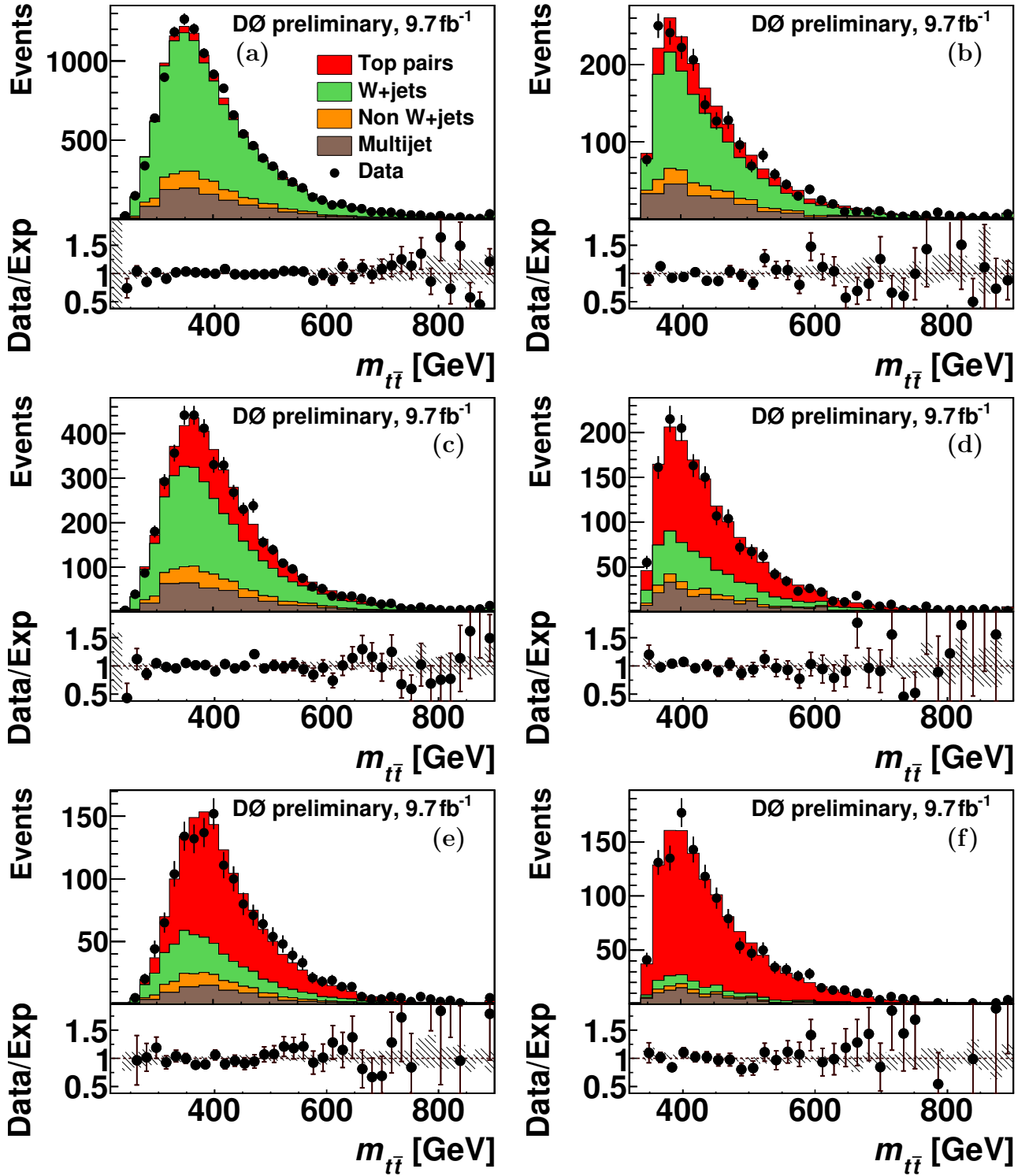


FIG. 4: Reconstructed invariant mass of the top quark–antiquark pair,  $m_{t\bar{t}}$ . The left column displays  $l+3$ jet events, and the right column displays  $l+\geq 4$ jet events. Rows from top to bottom display events with 0, 1, and  $\geq 2$   $b$  tags. The ratio between the data counts and the model expectation is shown in the lower panel, with the hashed area representing the systematic uncertainties.

For the 2D measurement, we use six  $m_{t\bar{t}}$  bins at the production level, with edges at 0, 400, 450, 500, 550, 650 and  $+\infty$  GeV. The joint distribution of  $\Delta y$  and  $m_{t\bar{t}}$  has a kinematic boundary at:  $|\Delta y| = \log([1 + \beta] / [1 - \beta])$ , where  $\beta = \sqrt{1 - (2m_t/m_{t\bar{t}})^2}$  and  $m_t$  is the mass of a top quark. Having a bin edge close to this boundary would result in a large difference in the event density between adjacent bins, a feature that would be smoothed by a regularization procedure, thus biasing  $u$ . To avoid such a bias, the  $\Delta y$ -edges of the bins of the 2D measurement were chosen to depend on  $m_{t\bar{t}}$  as shown in Fig 5.

The reconstruction-level histograms have similar but finer bins along both the  $\Delta y$  and  $m_{t\bar{t}}$  directions. In the  $l+3$  jet channels thirteen  $m_{t\bar{t}}$  bins are used, to accurately describe migrations among the six production-level bins. The  $m_{t\bar{t}}$  resolution in the  $l+\geq 4$  jet channels allows for fourteen  $m_{t\bar{t}}$  bins.

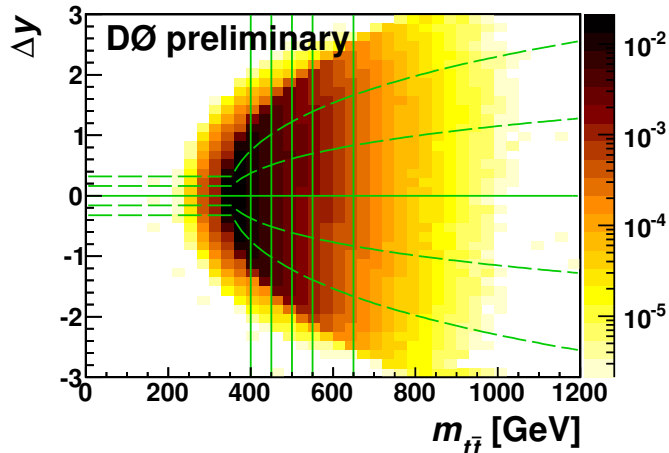


FIG. 5: Production-level bins for the 2D measurement in the  $(m_{t\bar{t}}, \Delta y)$  plane, overlaid on the distribution in these variables predicted from  $\text{MC@NLO}$ . The solid and dashed lines denote the production-level bins. The solid lines show bins that are used for the final result.

We simultaneously unfold the four channels that contain at least one  $b$  tag to the production level. The difference in purity among channels is accounted for in the definition of the covariance error matrix  $\mathbf{V}$ .

The unfolding technique is calibrated, and the statistical and systematical uncertainties are determined using the results of ensemble tests. Each ensemble comprises of simulated pseudo-datasets that we build according to  $\text{MC@NLO}$ , ALPGEN [31] or MADGRAPH [41] SM predictions, or according to toy models with different asymmetries. The pseudo-datasets are created from the expected bin counts  $\tilde{d}_i$  calculated using Eq. 4 by adding Poisson (statistical) and Gaussian (systematic) fluctuations, with the Gaussian width taken as one standard deviation for the corresponding systematic uncertainty.

In the toy models the input distribution  $P(\Delta y)$  has the form:

$$P(\Delta y) = G(\Delta y; \mu, w\sigma_0) (1 + \alpha \operatorname{erf}(\Delta y/\beta)), \quad (8)$$

where  $G$  is a Gaussian distribution with mean  $\mu$  and a width scaled by  $w$  from the  $\text{MC@NLO}$  predicted one of  $\sigma_0$ , and  $\alpha$  and  $\beta$  are shaping parameters. The shape of the  $\Delta y$  distribution and the input asymmetry are varied using the parameters  $\mu$ ,  $\alpha$ ,  $\beta$ , and  $w$ . In addition, we produce ensembles with the signal taken from simulated samples of  $t\bar{t}$  production mediated by axiglucos, hypothetical massive particles that arise in extensions of the SM that suggest different strong couplings for left and right handed quarks [8]. The input asymmetry in the models used for calibration ranges from -30% to +30%, while the axiglucos masses are varied from 0.2 to 2 TeV.

The bias, which is the average difference between the unfolded and simulated  $A_{\text{FB}}$  values, is shown in Fig. 6 as a function of the simulated  $A_{\text{FB}}$  value. Based on this study we derive a correction (calibration) that is applied to the result to eliminate the expected bias. The majority of the tested models are contained within the systematic uncertainty assigned to this calibration, which is shown by the dotted lines in Fig. 6. The one point that is significantly outside of the boundaries of this region corresponds to  $t\bar{t}$  production mediated by an axiglucos with a mass of 0.4 TeV. This particular model exhibits a significant change in  $A_{\text{FB}}$  on the  $m_{t\bar{t}}$  scale smaller than the bin width (here, 50 GeV), thus breaking the assumption of a smooth underlying distribution, leading to biased results. Since this behavior is common to all regularized unfolding procedures that bin their input distributions, we choose not to assign a systematic uncertainty that covers a specific class of models with rapidly changing  $A_{\text{FB}}$ . No systematic correlation is found between the biases in different  $m_{t\bar{t}}$  bins, which are therefore calibrated individually.

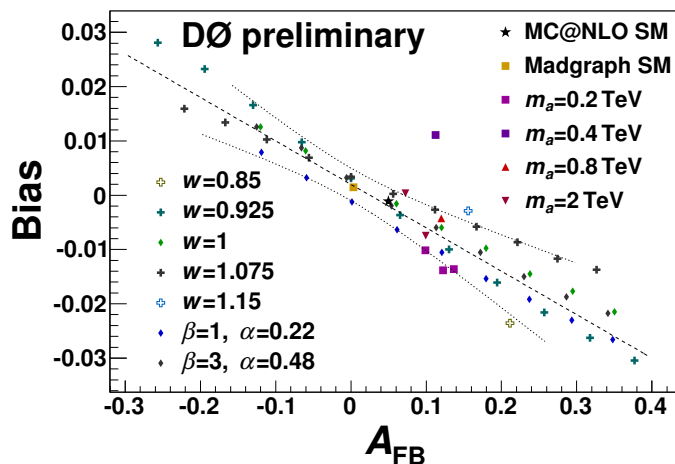


FIG. 6: The bias as a function of the simulated  $A_{FB}$ . Axigluon scenarios are indicated in the legend by the mass of the axigluon,  $m_a$ . The toy models are labeled by parameters  $w$ ,  $\alpha$  and  $\beta$  of Eq. 8. Unless stated otherwise  $w = 1$ ,  $\alpha = 0$  and  $\beta = 1$ . For each set of  $\alpha$ ,  $\beta$ , and  $w$  the value of  $\mu$  is varied to produce different input asymmetries. The dashed line indicates the calibration applied to the inclusive measurement and the dotted lines indicate the assigned calibration uncertainties.

## VII. SYSTEMATIC UNCERTAINTIES

The systematic uncertainties on the reconstruction- and production-level  $A_{FB}$  are summarized in Table IV in several broad categories, which are detailed below. To evaluate the systematic uncertainty on the reconstruction-level  $A_{FB}$  we vary the modeling according to the estimated uncertainty in the relevant parameter of the model, and propagate the effect to the result. The systematic uncertainties on the production-level  $A_{FB}$  are evaluated by including the effects of systematic variations on the simulated background-subtracted pseudo-data into the ensemble tests. The ensemble testing readily finds the total uncertainties on the measured  $A_{FB}$  values. The expected uncertainty due to each category is estimated using dedicated ensembles generated without statistical fluctuations and with only the relevant systematic effects.

TABLE IV: Systematic uncertainties on  $A_{FB}$ , in absolute %. For the 2D measurement, the range of changes in  $A_{FB}$  over the six  $m_{t\bar{t}}$  bins is given.

Source	Reco. level inclusive	Production level inclusive	2D
Background model	+0.7/−0.8	1.0	1.1–2.8
Signal model	< 0.1	0.5	0.8–5.2
Unfolding	N/A	0.5	0.9–1.9
PDFs and pileup	0.3	0.4	0.5–2.9
Detector model	+0.1/−0.3	0.3	0.4–3.3
Sample composition	< 0.1	< 0.1	< 0.1
Total	+0.8/−0.9	1.3	2.1–7.5

The **background model** category includes the following sources, which affect the properties predicted for background events. The leptonic asymmetry of the  $W$ +jets background is varied within its uncertainty of 3% [10]. The rate of heavy-flavor production within  $W$ +jets production is varied by 20% [36, 42]. The efficiencies for lepton identification, and the probabilities for a jet to be misidentified as a lepton, taken as functions of lepton momentum, are varied within their uncertainties to account for the uncertainty on the number of background events from multijet production [34]. This variation affects both the background shape and normalization. Uncertainties associated with the modeling of the discriminant and potentially increased background levels at high lepton pseudorapidity are also quantified by modifying the background model [10].

The **signal model** category includes the sources of uncertainty that affect the properties predicted for signal events other than the ones accounted for in the PDFs and pileup category. The top quark mass is varied according to the combined measurement of Ref. [43]. The effect of higher order corrections to  $t\bar{t}$  production is estimated by replacing

the migration matrix  $\mathbf{M}$  from Eq. 4 simulated by MC@NLO with the one simulated by ALPGEN, which uses tree-level matrix elements. The fragmentation functions are varied within their uncertainties, which also affects background modeling.

The signal model category also includes the uncertainties associated with the gluon radiation. The total amount of initial state radiation is varied in a range compatible with the results of Ref. [44]. We also consider the difference in the predicted amount of initial state radiation between forward and backward events, both because of contributions at order  $\alpha_s^3$  and due to higher order effects which are modeled by the simulated parton showers [45]. We account for this uncertainty by reducing the difference in the distributions of the  $p_T$  of the  $t\bar{t}$  system for forward and backward events by 25%, a value derived from Ref. [45]. We also account for the possibility that the mismodeling of this variable in the  $l+3$  jet final state affects  $A_{\text{FB}}$  by reweighting this distribution to match the D0 data, similarly to the procedure used in Ref. [10].

The uncertainties due to **unfolding** are dominated by the calibration uncertainties. The uncertainties associated with the choice of the regularization strength and statistical fluctuations in the MC samples used to find the migration matrix are also included.

The **PDFs and pileup** category includes uncertainties on the modeling of the  $p\bar{p}$  collisions. The main uncertainties are from the PDFs, which primarily affect the  $\Delta y$  distribution of the  $W$ +jets background. These uncertainties are evaluated by varying the contributions of the various eigenvectors from the CTEQ6.1 PDF [33] and by considering an alternative set of PDFs (MRST2003 [46]). The amount of additional collisions within the same bunch crossing (pile up) affects the quality of the reconstruction. The uncertainties on the modeling of additional collisions are also included in this category.

The **detector model** category includes the following sources of systematic uncertainty. The efficiencies of the  $b$ -tagging algorithm for jets of different flavors, which are measured from collider data, are varied according to their uncertainties. These variations affect the measured  $A_{\text{FB}}$  mostly through the estimated sample composition, which depends strongly on the classification of data into several channels according to the number of  $b$  tags. The modeling of jet energy reconstruction, including the overall energy scale and the energy resolution, as well as jet-reconstruction efficiencies and single-particle responses, are all calibrated to collider data and are varied according to their uncertainties. The uncertainties due to jet reconstruction and energy measurement are significantly reduced compared to the previous measurement due to the inclusion of the  $l+3$  jet events.

Lastly, the **sample composition** is varied according to its fitted uncertainties. This variation is in addition to the changes in the sample composition implicitly induced by other systematic variations.

## VIII. RESULTS

The calibrated production-level results are listed in Table V. The  $A_{\text{FB}}$  dependence on  $m_{t\bar{t}}$  is shown in Fig. 7 with the correlation factors between bins listed in Table VI.

TABLE V: Production-level asymmetries. The measured values are calibrated and listed with their total uncertainties. The theoretical predictions are based on MC@NLO simulation.

$m_{t\bar{t}}$ , GeV	$A_{\text{FB}},\%$	
	Predicted	Measured
< 400	2.2	$7.0 \pm 5.1$
400–450	4.6	$9.3 \pm 5.0$
450–500	6.7	$12.7 \pm 5.7$
500–550	8.4	$16.6 \pm 8.2$
550–650	10.9	$37.6 \pm 19.0$
> 650	14.8	$-12.3 \pm 29.6$
Inclusive	5.0	$10.6 \pm 3.0$

The values of the asymmetry measured in six  $m_{t\bar{t}}$  ranges constitute a six-dimensional vector  $\vec{v}$  with a 6x6 covariance matrix  $\Sigma$ . Table VII lists the eigenvectors  $\vec{b}_i$  ( $i = 1, \dots, 6$ ) of  $\Sigma$  together with the corresponding components of the vector  $\vec{v}$  in the basis formed by the eigenvectors:  $v_i = \vec{v} \cdot \vec{b}_i$ , and their uncertainties  $\sigma_i = \sqrt{\Sigma'_{ii}}$ , where  $\Sigma'$  is the covariance matrix transformed to the basis  $\vec{b}_i$ . The elements of Table VII fully specify the measured six-dimensional likelihood in the Gaussian approximation, and can be used for quantitative comparison with theoretical predictions and other experimental results [47].

Using the full covariance matrix we perform a fit of the measured  $A_{\text{FB}}$  to the functional form  $A_{\text{FB}}(m_{t\bar{t}}) = a + (\frac{m_{t\bar{t}}}{\text{GeV}} - C)b$ . We choose  $C = 445$  so that the correlation factor between the fit parameters  $a$  and  $b$  is less than 0.01 in

TABLE VI: The correlation factors between the measured  $A_{\text{FB}}$  values of the 2D measurement. All masses are in GeV.

	$m_{t\bar{t}}$ range (GeV)					
	< 400	400–450	450–500	500–550	550–650	> 650
< 400	+1.00	+0.89	+0.39	-0.19	-0.25	+0.12
400–450	+0.89	+1.00	+0.67	+0.10	-0.32	+0.12
450–500	+0.39	+0.67	+1.00	+0.68	-0.27	+0.05
500–550	-0.19	+0.10	+0.68	+1.00	+0.04	-0.12
550–650	-0.25	-0.32	-0.27	+0.04	+1.00	-0.41
> 650	+0.12	+0.12	+0.05	-0.12	-0.41	+1.00

TABLE VII: The eigenvectors of the covariance matrix  $\Sigma$  and the result of the 2D measurement  $\vec{v}$ , in the basis of eigenvectors.

$i$	Eigenvector $\vec{b}_i$	$v_i \pm \sigma_i$
1	(-0.592 +0.770 -0.237 -0.007 +0.004 -0.000)	0.000 $\pm$ 0.011
2	(+0.434 +0.099 -0.775 +0.448 -0.030 +0.002)	0.004 $\pm$ 0.021
3	(+0.673 +0.591 +0.251 -0.339 +0.138 -0.004)	0.130 $\pm$ 0.071
4	(+0.034 +0.192 +0.516 +0.826 +0.104 +0.049)	0.256 $\pm$ 0.093
5	(-0.076 -0.099 -0.113 -0.040 +0.917 +0.360)	0.265 $\pm$ 0.166
6	(-0.029 -0.030 -0.019 +0.031 +0.359 -0.932)	0.247 $\pm$ 0.311

the fit to the data. The parameters of the fit are listed in Table VIII for the data and the MC@NLO-based simulation. We observe a slope  $b$  consistent with zero and with MC@NLO prediction. The difference between the slopes reported in Ref. [3] and in this note corresponds to 1.8 standard deviations.

TABLE VIII: Parameters of the fit to  $A_{\text{FB}}(m_{t\bar{t}}) = a + (\frac{m_{t\bar{t}}}{\text{GeV}} - C)b$  with  $C = 445$ . The theoretical predictions are based on the MC@NLO simulation and have negligible statistical uncertainties.

Parameter	Predicted	Measured
$a$	$5.3 \cdot 10^{-2}$	$(11.9 \pm 3.6) \cdot 10^{-2}$
$b$	$3.8 \cdot 10^{-4}$	$(3.9 \pm 4.4) \cdot 10^{-4}$

## IX. DISCUSSION

The measured inclusive forward–backward asymmetry in  $t\bar{t}$  production,  $(10.6 \pm 3.0)\%$ , as well as the asymmetry dependence on the invariant mass of the  $t\bar{t}$  system are in the agreement with the SM predictions reviewed in Section IV that range from an inclusive asymmetry of 5.0% predicted by the MC@NLO-based simulation to  $8.8 \pm 0.9\%$  [25] once the electroweak effects are taken into account.

To quantify the consistency of the presented result with the one published in Ref. [4], Table IX presents  $A_{\text{FB}}$  at the reconstruction level measured in different samples. The method discussed in this note applied to  $l+\geq 4$  jet events from the first  $5.4 \text{ fb}^{-1}$  of data yields a result consistent with that in Ref. [4], but with a reduced uncertainty mainly due to the separation of data into channels based on the number of  $b$  tags. Once the analysis is extended to include the  $l+3$  jet events collected at that time, the uncertainty is reduced by a factor of 1.26. The result obtained in the second  $4.3 \text{ fb}^{-1}$  of the Tevatron data is statistically consistent with that obtained in the first  $5.4 \text{ fb}^{-1}$ . The statistical uncertainty obtained in the combined  $9.7 \text{ fb}^{-1}$  of data is reduced by a factor of 1.29 with respect to the result obtained using the same method in  $5.4 \text{ fb}^{-1}$ , while the reduction expected from scaling with the integrated luminosity is 1.34. This loss of sensitivity is mainly due to higher instantaneous luminosity during the collection of the later data, which required a tighter trigger selection.

The improved reconstruction of  $\Delta y$  results in further reduction of the statistical uncertainty on the unfolded result compared to Ref. [4] since it lowers the probability for events to migrate between the forward and backward categories. The separation of the data into channels allows us to add the purer  $l+3$  jet channels without losing the statistical power of the purer  $l+\geq 4$  jet channels.

TABLE IX: Reconstruction-level asymmetries measured in different samples with different methods, with their statistical uncertainties.

Sample	Method	Reco-level $A_{FB}$ , %
$l+\geq 4$ jet, first $5.4 \text{ fb}^{-1}$	From Ref. [4]	$9.2 \pm 3.7$
$l+\geq 4$ jet, first $5.4 \text{ fb}^{-1}$	This analysis	$9.9 \pm 3.4$
$l+\geq 3$ jet, first $5.4 \text{ fb}^{-1}$	This analysis	$10.1 \pm 2.7$
$l+\geq 3$ jet, additional $4.3 \text{ fb}^{-1}$	This analysis	$6.0 \pm 3.1$
$l+\geq 3$ jet, full $9.7 \text{ fb}^{-1}$	This analysis	$7.9 \pm 2.1$

## X. SUMMARY

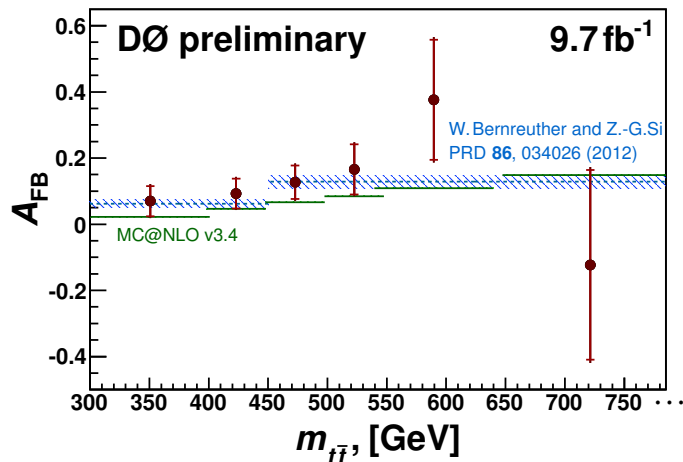


FIG. 7: The dependence of the forward-backward asymmetry on the invariant mass of the  $t\bar{t}$  system. The points are the D0 data with the total error bars indicating the total uncertainty, based on the diagonal elements of the covariance matrix, while the statistical uncertainties are indicated by the inner error bars. The horizontal lines show MC@NLO-based SM prediction [24]. Shaded boxes correspond to the prediction of Refs. [22, 25]. The last bin has no upper boundary.

We report on the measurement of the forward-backward asymmetry in  $t\bar{t}$  production using the dataset recorded by the D0 detector in Run II of the Fermilab Tevatron Collider. The results presented here supersede the ones that were based on about half of the data [4]. The analysis is extended to include events with three jets, allowing for the loss of one jet from the  $t\bar{t}$  decay and reducing the acceptance corrections. The unfolding procedure now accounts for the differences in sample compositions between channels, thus maximizing the statistical strength of the individual channels. New reconstruction techniques are used in the  $l+\geq 4$  jet channel, improving the experimental resolution in all variables of interest.

The asymmetry measured at the reconstruction level is  $(7.9 \pm 2.1(\text{stat})_{-0.9}^{+0.8}(\text{syst}))\%$ . After correcting for detector resolution and acceptance, we obtain an asymmetry of  $(10.6 \pm 3.0)\%$ . The observed asymmetry and the dependence of  $A_{FB}$  on  $m_{t\bar{t}}$  are consistent with the standard model predictions.

## Acknowledgments

We thank M. Mangano, P. Skands and G. Perez for enlightening discussions. We thank the staffs at Fermilab and collaborating institutions, and acknowledge support from the DOE and NSF (USA); CEA and CNRS/IN2P3 (France); FASI, Rosatom and RFBR (Russia); CNPq, FAPERJ, FAPESP and FUNDUNESP (Brazil); DAE and DST (India); Colciencias (Colombia); CONACyT (Mexico); KRF and KOSEF (Korea); CONICET and UBACyT (Argentina); FOM (The Netherlands); STFC and the Royal Society (United Kingdom); MSMT and GACR (Czech Republic); CRC Program and NSERC (Canada); BMBF and DFG (Germany); SFI (Ireland); The Swedish Research

Council (Sweden); and CAS and CNSF (China).

- 
- [1] V. M. Abazov *et al.* (D0 Collaboration), Phys. Rev. Lett. **100**, 142002 (2008).
- [2] T. Aaltonen *et al.* (CDF Collaboration), Phys. Rev. Lett. **101**, 202001 (2008).
- [3] T. Aaltonen *et al.* (CDF Collaboration), Phys. Rev. D **83**, 112003 (2011).
- [4] V. Abazov *et al.* (D0 Collaboration), Phys. Rev. D **84**, 112005 (2011).
- [5] CMS Collaboration, Phys. Rev. D **87**, 092002 (2013).
- [6] J. H. Kuhn and G. Rodrigo, Phys. Rev. Lett. **81**, 49 (1998).
- [7] L. G. Almeida, G. Sterman, and W. Vogelsang, Phys. Rev. D **78**, 014008 (2008);  
M. T. Bowen, S. D. Ellis, and D. Rainwater, Phys. Rev. D **73**, 014008 (2006);  
S. Dittmaier, P. Uwer, and S. Weinzierl, Phys. Rev. Lett. **98**, 262002 (2007);  
K. Melnikov and M. Schulze, Nucl. Phys. B **840**, 129 (2010);  
J. H. Kuhn and G. Rodrigo, JHEP **1201** 063 (2012).
- [8] P. H. Frampton and S. L. Glashow, Phys. Lett. B **190** 157 (1987).
- [9] Y. Cui, Z. Han and M. D. Schwartz, JHEP **1107** 127 (2011).
- [10] V. M. Abazov *et al.* [D0 Collaboration], submitted to Phys. Rev. D, arXiv:1403.1294[hep-ex].
- [11] R. Demina, A. Harel and D. Orbaker, arXiv:1310.3263.
- [12] V. M. Abazov *et al.* (D0 Collaboration), Nucl. Instrum. Methods Phys. Res. A **620**, 490 (2010).
- [13] V. M. Abazov *et al.* (D0 Collaboration), Nucl. Instrum. Meth. A **565**, 463 (2006);  
R. Angstadt *et al.* (D0 Collaboration), Nucl. Instrum. Meth. A **622**, 298 (2010).
- [14] S. Abachi *et al.* (D0 Collaboration), Nucl. Instrum. Methods Phys. Res. A **338**, 185 (1994).
- [15] V. M. Abazov *et al.* (D0 Collaboration), Nucl. Instrum. Methods Phys. Res. A **552**, 372 (2005).
- [16] M. Abolins *et al.*, Nucl. Instrum. Methods in Phys. Res. Sect. A **584**, 75 (2008).
- [17] S. Snyder, “*Measurement of the Top Quark mass at D0*”, Doctoral Thesis, State University of New York at Stony Brook (1995).
- [18] B. A. Betchart, R. Demina and A. Harel, Nucl. Instrum. Meth. A **736**, 169 (2014).
- [19] I. Volobouev, arXiv:1101.2259 (2011).
- [20] V. Abazov *et al.* (D0 Collaboration), Phys. Rev. D **85**, 051101 (2012).
- [21] A. Hoecker, P. Speckmayer, J. Stelzer, J. Therhaag, E. von Toerne, and H. Voss, “TMVA: Toolkit for Multivariate Data Analysis,” PoS A CAT 040 (2007) [physics/0703039].
- [22] Private communications with W. Bernreuther, updating the error estimates of Ref. [25].
- [23] M. Czakon, P. Fiedler, A. Mitov, CERN-PH-TH-2013-056, TTK-13-08, arXiv:1303.6254.
- [24] S. Frixione and B. R. Webber, JHEP **0206** 029 (2002);  
S. Frixione, P. Nason and B. R. Webber, JHEP **0308** 007 (2003).
- [25] W. Bernreuther and Z.-G. Si, Phys. Rev. D **86** 034026 (2012), and references therein.
- [26] e.g., L. G. Almeida, G. F. Sterman and W. Vogelsang, Phys. Rev. D **78** 014008 (2008);  
N. Kidonakis, Phys. Rev. D **84** 011504 (2011).
- [27] J. M. Campbell and R. K. Ellis, arXiv:1204.1513 [hep-ph] (2012).
- [28] S. J. Brodsky and X.-G. Wu, Phys. Rev. D **85** 114040 (2012);  
X.-G. Wu, S. J. Brodsky and M. Mojaza, arXiv:1302.0599;  
S. J. Brodsky, M. Mojaza and X.-G. Wu, arXiv:1304.4631.
- [29] S. J. Brodsky, Annu. Rev. Nucl. Part. Sci. **2012.62** 1-13 (2012).
- [30] G. Corcella *et al.*, J. High Energy Phys. **01**, 010 (2001).
- [31] M. L. Mangano *et al.*, hep-ph/0206293, CERN-TH-2002-129 (2002).
- [32] T. Sjöstrand *et al.*, Comput. Phys. Commun. **135**, 238 (2001).
- [33] D. Stump *et al.*, JHEP **0310** 046 (2003).
- [34] V. M. Abazov *et al.* (D0 Collaboration), Phys. Rev. D **84**, 012008 (2011).
- [35] E. Boos *et al.* [CompHEP Collaboration], Nucl. Instrum. Meth. Sect. A **534**, 250 (2004).
- [36] J. M. Campbell and R. K. Ellis, Nucl. Phys. Proc. Suppl. **205**, 10 (2010).
- [37] G. Hanson *et al.* Phys.Rev.Lett **35**, 1609 (1975).
- [38] F. Abe *et al.* (CDF Collaboration), Phys.Rev.Lett **81**, 5754 (1998).
- [39] <http://root.cern.ch/root/html/TUnfold.html> and reference within.  
In particular: <http://www.desy.de/~sschmitt> and  
P. C. Hansen, in Computational Inverse Problems in Electrocardiology, ed. P. Johnston, Advances in Computational Bioengineering (2000), <http://www.imm.dtu.dk/~pch/TR/Lcurve.ps>
- [40] G. Bohm and G. Zech, “*Introduction to Statistics and Data Analysis for Physicists*”, Verlag Deutsches Elektronen-Synchrotron, <http://www-library.desy.de/elbook.html> (2010).
- [41] J. Alwall *et al.*, JHEP **1106** 128 (2011).
- [42] V. M. Abazov *et al.* [D0 Collaboration], Phys. Rev. D **84**, 012008 (2011).
- [43] T. Aaltonen *et al.* [CDF and D0 Collaborations], Phys. Rev. D **86**, 092003 (2012).

- [44] V. M. Abazov *et al.* (D0 Collaboration), Phys. Rev. Lett. **106**, 122001 (2011).
- [45] P. Skands, B. Webber and J. Winter, JHEP **1207**, 151 (2012);  
J. Winter, P. Z. Skands and B. R. Webber, EPJ Web Conf. **49**, 17001 (2013).
- [46] A. D. Martin, R. G. Roberts, W. J. Stirling and R. S Thorne, Eur. Phys. J. **C35** 325 (2004).
- [47] G. Zech, in *Proceedings of the PHYSTAT 2011 Workshop on Statistical Issues Related to Discovery Claims in Search Experiments and Unfolding*, 10.5170/CERN-2011-006 (2011).